

# Causal Graph Recovery in Neuroimaging through Answer Set Programming

Anonymous Submission

## Abstract

Learning graphical causal structures from time series data presents significant challenges, especially when the measurement frequency does not match the causal timescale of the system. This often leads to a set of equally possible underlying causal graphs due to information loss from sub-sampling (i.e., not observing all possible states of the system throughout time). Our research addresses this challenge by incorporating the effects of sub-sampling in the derivation of causal graphs, resulting in more accurate and intuitive outcomes. We use a constraint optimization approach, specifically answer set programming (ASP), to find the optimal set of answers. ASP not only identifies the most probable underlying graph, but also provides an equivalence class of possible graphs for expert selection. In addition, using ASP allows us to leverage graph theory to further prune the set of possible solutions, yielding a smaller, more accurate answer set significantly faster than traditional approaches. We validate our approach on both simulated data and empirical structural brain connectivity, and demonstrate its superiority over established methods in these experiments. We further show how our method can be used as a meta-approach on top of established methods to obtain, on average, 12% improvement in F1 score. In addition, we achieved state of the art results in terms of precision and recall of reconstructing causal graph from sub-sampled time series data. Finally, our method shows robustness to varying degrees of sub-sampling on realistic simulations, whereas other methods perform worse for higher rates of sub-sampling.

## 1 Introduction

Causal inference from functional Magnetic Resonance Imaging (fMRI) data has emerged as a critical endeavor to understand the neural mechanisms underlying cognitive processes and behaviors. Researchers not only seek to identify active brain regions during tasks, but also unravel the causal relationships between these regions, often referred to as "effec-

tive connectivity" [Friston, 1994]. Graphical causal models, such as causal Bayesian networks, have become a popular framework for this purpose, combining directed graphs with joint probability distributions to model the dependencies between different brain regions [Pearl, 2009]. These models adhere to the Causal Markov Condition, which asserts that each node in a causal graph is conditionally independent of its non-descendants given its parents [Spirtes *et al.*, 2001].

However, applying these models to fMRI data is fraught with challenges, particularly due to the mismatch between the temporal resolution of fMRI and the rapid timescale of neural processes. The typical sampling intervals in fMRI, ranging from one to three seconds, are much slower than the millisecond-level interactions between neurons, leading to significant undersampling [Valdes-Sosa *et al.*, 2011]. This undersampling often results in the identification of multiple causal graphs that are statistically indistinguishable, forming what is known as a Markov Equivalence Class [Pearl, 2009; Spirtes *et al.*, 2001]. These problems are exacerbated by the indirect nature of the BOLD signal, which reflects neural activity through complex and variable hemodynamic responses [Handwerker *et al.*, 2004].

In addition, the inherent variability in the hemodynamic response across different brain regions and subjects, adds another layer of complexity. Variations in the time-to-peak of the BOLD response can lead to incorrect inferences about the direction of causality, particularly when using methods like Granger causality, which assumes a fixed temporal relationship between cause and effect [David *et al.*, 2008; Seth *et al.*, 2013]. Although some studies suggest that Granger causality may be robust to certain variations in the hemodynamic response [Seth *et al.*, 2013], the combination of measurement noise, undersampling, and hemodynamic variability often undermines the reliability of causal inferences from fMRI data.

In response to these challenges, this paper proposes a novel approach that explicitly accounts for the effects of undersampling in the derivation of causal graphs. By employing constraint optimization through state-of-the-art Answer Set Programming (ASP), we aim to identify the most probable causal graph from a set of potential candidates. ASP allows for the incorporation of domain-specific knowledge and constraints, facilitating the identification of not only a single graph but an equivalence class of possible graphs, thereby offering a more

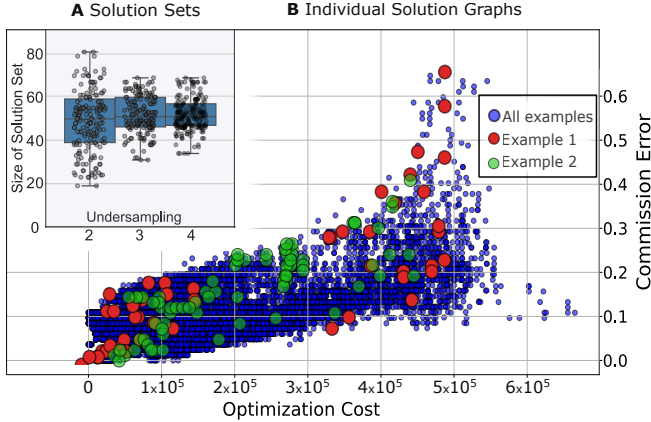


Figure 1: Top left(A): Size of optimization solution set across different undersamplings, repeated 100 times. Bottom right(B): Commission error of the solution vs. optimization cost for that solution. Solutions in one equivalent class are highlighted in red.

comprehensive understanding of the underlying causal structure [Gebser *et al.*, 2012].

Furthermore, we introduce a method to enhance the robustness and accuracy of causal inference by integrating data from multiple instances of the same underlying causal system, such as combining fMRI data from several subjects performing the same task. This approach synthesizes information across these instances into a singular causal graph, leveraging ASP's ability to handle complex combinatorial problems that would otherwise be infeasible with conventional techniques [Lifschitz *et al.*, 2008].

We validate our approach using both simulated data and real fMRI data from macaque brains, demonstrating its superiority over existing methods [Smith *et al.*, 2011; Ramsey *et al.*, 2010]. Our results suggest that ASP offers a powerful new tool for causal inference in neuroimaging, providing more accurate and intuitive insights into the brain's functional architecture.

## 2 Background

Causal inference from time series data, particularly from fMRI, has been a central focus in computational neuroscience due to its potential to uncover complex neural mechanisms. A directed dynamic causal model extends standard causal models [Pearl and others, 2000; Spirtes *et al.*, 1993] by incorporating temporal dependencies, where the graph  $\mathbf{G}$  includes nodes representing random variables  $\mathbf{V} = \{V_1, V_2, \dots, V_n\}$  across both the current timestep  $t(\mathbf{V}^t)$  and previous timesteps  $(\mathbf{V}^{t-k})$  that are direct causes of some  $V_i^t$ . These models assume a first-order Markov structure, where  $\mathbf{V}^t$  is conditionally independent of  $\mathbf{V}^{t-k}$  given  $\mathbf{V}^{t-1}$  for all  $k > 1$ , allowing flexibility in the causal timescale [Spirtes *et al.*, 2000].

Undersampling presents a significant challenge in fMRI, where data is collected at intervals longer than the timescale of underlying neural processes. If the true causal structure evolves over timepoints  $\{t^0, t^1, t^2, \dots, t^k, \dots\}$ , but measurements are taken at  $\{t^0, t^u, t^{2u}, \dots, t^{ku}, \dots\}$ , this results in an undersampled graph  $\mathbf{G}^u$  that may obscure the true causal

graph  $\mathbf{G}^1$  [Danks and Plis, 2013; Gong *et al.*, 2015].

To address the structural implications of undersampling, several approaches have been developed. For instance, Danks and Plis [2013] explored the problem structurally, while Gong *et al.* [2015] provided a parametric approach for two-variable systems. The resulting undersampled graphs are typically compressed, with temporal information encoded in the edges. Specifically: (1) In the undersampled graph  $\mathcal{G}^u$ , an edge  $V_i \rightarrow V_j$  exists if and only if there is a directed path of length  $u$  from  $V_i$  to  $V_j$  in the fully observed graph  $\mathcal{G}^1$ , or equivalently, if there exists a directed path from  $V_i^{t-u}$  to  $V_j^t$  in  $\mathbf{G}^1$ . This property captures how dependencies persist across multiple timesteps despite undersampling. (2) Similarly, a bidirected edge  $V_i \leftrightarrow V_j$  in  $\mathcal{G}^u$  arises when there exists a common ancestor  $V_k$  in  $\mathcal{G}^1$  that has directed paths to both  $V_i$  and  $V_j$ , with the intermediate connections spanning fewer than  $u$  timesteps. This implies that  $V_k$  serves as an unobserved confounder, introducing dependencies that persist through undersampling.

Dealing with latent confounders, such as those introduced by undersampling, has led to the development of various graph representations, including Partially-Observed Ancestral Graphs (PAGs) [Zhang, 2008] and Maximal Ancestral Graphs (MAGs) [Richardson and Spirtes, 2002]. However, these frameworks often struggle with the complexities introduced by undersampling [Mooij and Claassen, 2020]. Compressed graphs have proven more effective in addressing the challenge of inferring the true causal graph  $\mathbf{G}^1$  from an observed graph  $\mathcal{H}$  under unknown undersampling rates.

The Rate-Agnostic Structure Learning (RASL) algorithm [Plis *et al.*, 2015] was introduced to address the challenge of causal inference from undersampled data, placing a strong emphasis on directly tackling undersampling while adopting a rate-agnostic approach that avoids assumptions about the undersampling rate. By systematically considering all possible rates and incorporating stopping rules to eliminate redundant graph exploration, RASL marked a significant advancement in computational efficiency. However, it faced practical limitations in scaling to larger graphs, leaving room for further improvement.

Building on these foundations, recent advancements in causal structure learning have led to the development of generalized rate-agnostic approaches that significantly enhance the scalability and efficiency of these methods. The reformulation of RASL into a constraint satisfaction framework, expressed using a declarative language, has shown considerable promise by enabling more efficient analysis of large graphs called Solver-based RASL (sRASL) [Abavisani *et al.*, 2023]. By incorporating additional constraints based on strongly connected components (SCC) structures, this approach provides a scalable and accurate solution for causal inference from undersampled data, capable of analyzing datasets with over 100 nodes—a substantial improvement over earlier methods that struggled with smaller graphs. The proposed sRASL method achieves a 1000-fold improvement in solving time, while maintaining the same theoretical guarantees as its predecessors. Nonetheless, sRASL exhibits limitations when applied to real-world datasets, particularly in

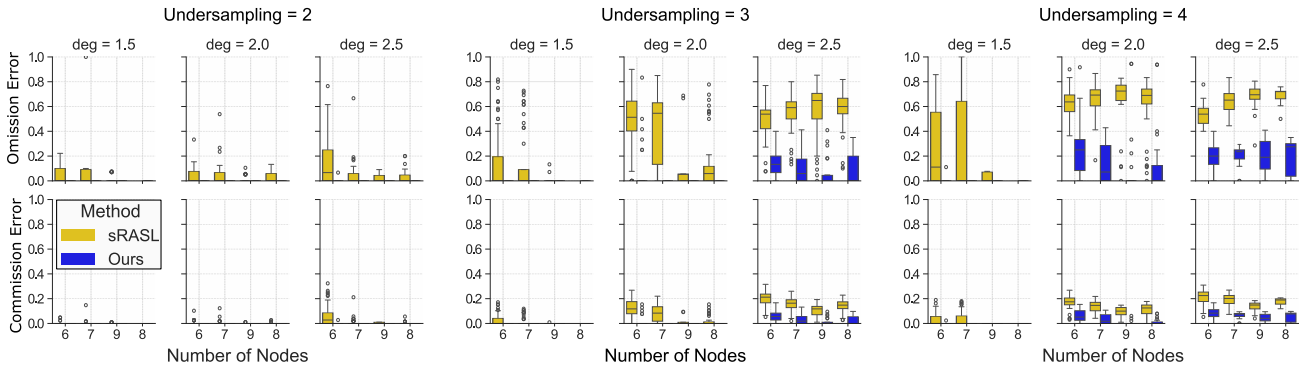


Figure 2: Normalized omission (top) and commission (bottom) errors for edge-breaking experiments with varying undersampling rates and graph densities, comparing the original approach with our improved sRASL-based method.

181 the presence of environmental noise, as its performance gains  
 182 observed in simulations do not fully translate to noisy, real-  
 183 world conditions.

184 In a comprehensive study by Sanchez-Romero *et al.*  
 185 [2019b], various statistical methods were assessed for their  
 186 effectiveness in recovering the causal structure of systems  
 187 with feedback from synthetic BOLD time series. The study  
 188 compared established methods, such as Granger causal re-  
 189 gression and multivariate autoregressive models, with newer  
 190 approaches like Fast Adjacency Skewness (FASK) and Two-  
 191 Step, both of which leverage non-Gaussian features of the  
 192 BOLD signal. Their analysis covered feedback structures, ex-  
 193 citatory and inhibitory feedback, and models using macaque  
 194 structural connectivity as well as human resting-state and  
 195 task data. Several methods demonstrated over 80% orienta-  
 196 tion precision and recall, including those involving 2-cycles.  
 197 However, this study did not account for the fact that BOLD  
 198 data is inherently undersampled. Therefore, in the current  
 199 article, we investigated how the algorithms studied in the  
 200 Sanchez-Romero paper track the structure of graphs with a  
 201 sparse sample and compared these algorithms with an algo-  
 202 rithm based on Answer Set Programming (ASP). The FASK  
 203 algorithm showed good results along with the ASP algorithm.

204 In recent years, causal discovery in fMRI has advanced  
 205 significantly, with new methods pushing the boundaries of  
 206 connectivity estimation by incorporating non-linearities, han-  
 207 dling latent confounders, and applying complex neural net-  
 208 work models. Methods such as LiNGAM [Shimizu *et al.*,  
 209 2006] are well-suited for identifying directed causal relation-  
 210 ships in linear, non-Gaussian acyclic models, making them  
 211 highly effective for discovering directed interactions within  
 212 complex neural networks. Other innovative approaches like  
 213 EC-GAN [Kim *et al.*, 2021] use generative adversarial frame-  
 214 works to infer effective connectivity, while models such as  
 215 the Amortization Transformer [Paul *et al.*, 2022] and rein-  
 216 forcement learning algorithms like ActorCritic [Mnih *et al.*,  
 217 2016] adapt dynamically to the intricate patterns of whole-  
 218 brain causal structures, as seen in CALLTiF [Salehi *et al.*,  
 219 2021] and DYNOTEARNS [Pamfil *et al.*, 2020].

220 However, for our study, we selected the methods from  
 221 Sanchez-Romero's work—GIMME [Gates and Molenaar,  
 222 2010], MVGC [Barnett and Seth, 2009], MVAR [Bressler and

Seth, 2003], and FASK [Sanchez-Romero *et al.*, 2019a]—as  
 223 the primary benchmarks for comparison. These methods  
 224 provide a robust, established foundation for causal infer-  
 225 ence in fMRI, especially in handling real-world challenges  
 226 such as feedback loops, individual variability, and multi-  
 227 variate time-series dependencies. GIMME is particularly  
 228 effective in capturing both individual and group-level con-  
 229 nectivity, essential for population studies, while MVGC and  
 230 MVAR offer reliable multivariate approaches for assessing  
 231 directional dependencies in time series data. FASK, on  
 232 the other hand, improves causal orientation accuracy by lever-  
 233 aging non-Gaussian characteristics, which are beneficial in  
 234 the context of noisy fMRI data. By comparing our method  
 235 with these well-established approaches, we aim to benchmark  
 236 against standard, validated techniques, allowing us to clearly  
 237 assess the relative strengths and limitations of our approach  
 238 in a field-relevant framework.

239 Building on these findings, we evaluated the performance  
 240 of these algorithms when applied to undersampled data,  
 241 benchmarking them against Answer Set Programming (ASP).  
 242 Our results offer new insights into the robustness and accu-  
 243 racy of these methods in the context of undersampling, a fre-  
 244 quent challenge in fMRI analysis.

### 3 Methods

246 In this study, we present an enhanced version of the sRASL  
 247 framework [Abavisani *et al.*, 2023] to improve its applicabil-  
 248 ity to functional brain connectivity analysis using fMRI data.  
 249 We call this new method Real-world noisy RASL or **RnR**  
 250 for short. The original sRASL was developed for structural graph  
 251 analysis, but was limited by its assumption of a single opti-  
 252 mal solution and lacked realism in recovered graph densities.  
 253 To address these limitations, we propose the following key  
 254 innovations:

- Optimization in OptN Mode: Using Clingo in OptN mode to retrieve all near-optimal solutions, enabling comprehensive exploration of equally valid solutions.
- Density Constraints: Introducing a density-matching constraint to ensure that the recovered graph reflects realistic functional brain connectivity.

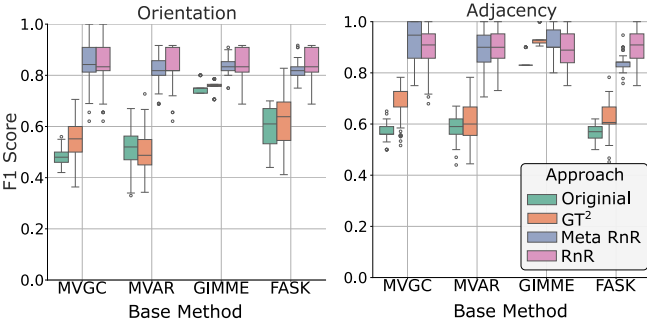


Figure 3: Performance comparison using Sanchez-Romero’s data with and without the RASL meta-solver. Applying RASL on top of traditional methods improves accuracy by accounting for undersampling effects, with additional gains achieved by using PCMCI.

- RnR as Meta Solver: We propose a general framework for using our method as a meta-solver (constraining other causal learning algorithms) to take into account effects of undersampling.
- Prioritized Optimization: Implementing a multi-stage optimization process that prioritizes graph density, followed by bidirectional and directed connections.
- Adaptive Weighting: Applying adaptive weighting schemes to improve graph accuracy by accounting for uncertainty in fMRI-derived connections.

These enhancements collectively enable the recovery of functional connectivity graphs that are both biologically realistic and also structurally accurate, while addressing challenges distinctive to fMRI data.

### 3.1 Overview of the sRASL Framework

The sRASL framework takes as input an undersampled graph  $\mathcal{H}$ , which can be derived from empirical data  $D$ , expert knowledge, or a combination of both. Its key principle relies on the modular structure of strongly connected components (SCCs), which must form a Directed Acyclic Graph (DAG). This structural constraint reduces the solution space by eliminating invalid graph configurations. In its original implementation, sRASL returned only a single optimal solution, limiting its ability to account for inherent noise in fMRI data. Additionally, the absence of density constraints led to unrealistic output graphs (in terms of connectivity densities).

### 3.2 Optimization in OptN Mode

In the original sRASL method, a single solution corresponding to the minimum cost function value was returned. This is restrictive because multiple solutions can have comparable costs, especially in noisy datasets like fMRI. To overcome this, we utilize Clingo in OptN mode, which retrieves all near-optimal solutions within a specified cost range. The optimization objective is defined as:

$$\begin{aligned} \mathcal{G}^* \in \arg \min & \left( \sum_{e \in \mathcal{H}} I[e \notin \mathcal{G}] \cdot w(e \in \mathcal{H}) \right. \\ & \left. + \sum_{e \notin \mathcal{H}} I[e \in \mathcal{G}] \cdot w(e \notin \mathcal{H}) \right) \end{aligned} \quad (1)$$

where the indicator function  $I(c) = 1$  if condition  $c$  holds, and 0 otherwise. The weights  $w(e \in \mathcal{H})$  and  $w(e \notin \mathcal{H})$  reflect the importance of edge presence or absence, respectively. By setting the OptN flag in Clingo, we retrieve all solutions within a practical cost range, enabling a more robust exploration of near-optimal graphs.

### 3.3 RnR as meta solver

A common challenge in causal learning is unobserved common causes. In the present context, if the common cause of two nodes is removed due to lower temporal resolution, then there will be bidirectional correlations between nodes, as described in Section 2. Many causal structure learning methods produce bidirected edges [Runge *et al.*, 2019; Granger, 1969; Lütkepohl, 2005], but methods that do not account for undersampling will not produce bidirected edges [Gates and Molenaar, 2010; Barnett and Seth, 2009; Bressler and Seth, 2003; Sanchez-Romero *et al.*, 2019a]. We present an approach where our method can be used as a meta-solver, thereby gaining the benefits of the chosen first-order method, while accommodating undersampling due to our method.

In addition, our empirical studies revealed that, when methods return a length-2 loop between two nodes, then there is always (i) a bidirected edge between them in the correct model, and (ii) one or both of the two directed edges. We thus add bidirected edges to the graph output by the first-order method. We also add both directed edges to the graph, though with low weight for each direction to encode uncertainty about which might be present. We thus have an enriched graph consisting of directed and bidirected edges for input to the RnR solver.

### 3.4 Density Constraint for Realistic Graphs

To ensure biological plausibility, we introduce a density constraint that keeps the connectivity density of the recovered graph close to that observed in real functional brain networks. Specifically, the total number of edges in the graph is constrained to be within a realistic range derived from empirical fMRI studies. This prevents solutions that are excessively dense or sparse, when compared to actual brain connectivity.

### 3.5 Prioritized Optimization by Connection Type

We implemented a multi-stage optimization process that prioritizes specific types of connections to ensure that broad structural characteristics (e.g., density and bidirectional edges) are recovered first, with finer details added in subsequent stages. The optimization first focuses on ensuring that the graph density matches the expected range. Once the density is matched, the algorithm prioritizes recovery of bidirectional connections, which are more likely to represent strong functional interactions, and are the more reliable constraints. In addition, bidirected edges provide important information

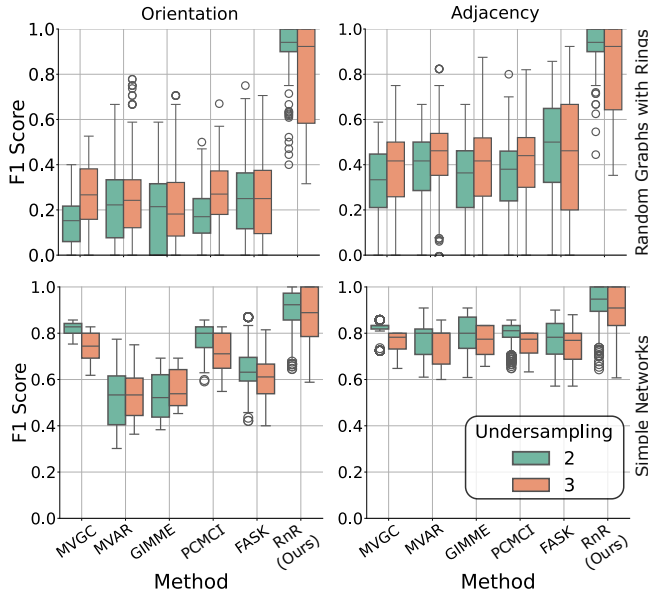


Figure 4: Comparison of Sanchez-Romero’s simple data generation approach with larger, more complex VAR-generated graphs. Sanchez-Romero’s data lacks real loops and is limited in scope, which may affect the generalizability of causal inference results.

framework achieves more accurate and realistic recovery of functional brain networks from fMRI data. These modifications address critical limitations in the original method, making it better suited for noisy and complex real-world applications.

## 4 Results

### 4.1 Improved Edge-Breaking Experiment

We replicated and extended the edge-breaking experiment from Abavisani et al. (2023), demonstrating the robustness of the sRASL approach when applied to graphs with intentionally broken edges. In this experiment, we generated a causal ground truth graph  $\mathcal{G}^1$  and undersampled it at various rates, simulating noise by randomly deleting an edge. The goal was to test the ability of sRASL to recover the true graph structure. Our results, depicted in Figure 2, show that sRASL consistently achieved lower omission and commission errors compared to the original approach, even under high undersampling conditions. This illustrates that sRASL can more effectively restore the true graph structure, making it robust against edge-breaking perturbations.

### 4.2 BOLD simulation data: Enhancing Causal Inference with RASL as a Meta-Solver

We further evaluated the sRASL approach on simulated data from Sanchez-Romero et al. (2019a). Dataset from Sanchez-Romero et al. (2019a), which is widely accepted within the Neuroscience community, was generated with small, simple graphs lacking real loops and using an idiosyncratic data generation method. We demonstrated that Sanchez-Romero’s existing methods do not account for the effects of undersampling, which can bias causal inference.

Our approach applied sRASL as a meta-solver: after running Sanchez-Romero’s original methods, we utilized sRASL on the resulting graph to incorporate the effects of undersampling explicitly. This adjustment led to improved accuracy, as sRASL optimized the causal graph structure to better reflect the underlying dynamics. In essence, sRASL served as an enhancement layer, correcting for undersampling effects ignored by previous methods (Figure 3).

Additionally, we explored the use of PCMCI as an alternative to standard methods like SVAR and Granger Causality (GC). In their 2017 study, Cook, Danks, and Plis demonstrated that SVAR and GC perform well for scenarios with isochronal bidirected edges, which arise due to undersampling, as well as directed edges. However, we observed that PCMCI, initially introduced by Moneta et al. and later significantly improved by Runge, performs better in these scenarios. Therefore, we incorporated PCMCI with RASL, achieving more accurate results by effectively handling undersampling and improving causal inference. Figure 3 illustrates these improvements.

### 4.3 Sanchez-Romero’s Simulation Data

### 4.4 Analyzing the Limitations of Sanchez-Romero’s Data Generation

Despite its widespread acceptance, Sanchez-Romero’s data generation approach is limited in scope and complexity. It

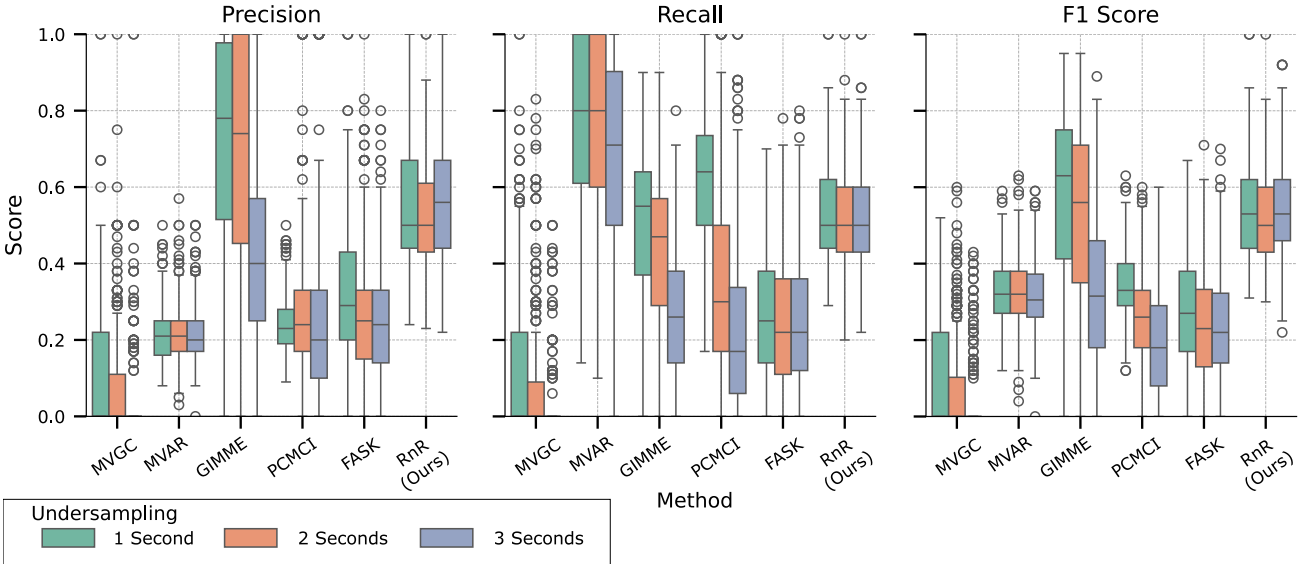


Figure 5: Impact of different undersampling rates (1s, 2s, 3s) on BOLD signal preservation in fMRI data simulated with the balloon model. Minimal error is observed with 1-second undersampling, whereas larger intervals degrade accuracy in all methods that don't account for undersampling effect. Our method RnR accounts for this effect and does not suffer loss from undersampling.

429 employs simple, small graphs without real loops and is generated using a specific, contrived process. To demonstrate  
430 the limitations of this dataset for broader causal inference applications, we conducted experiments with larger VAR models on graphs with many variables and more complex structures,  
431 showcasing the limitations of Sanchez-Romero's setup (Figure 4). This underscores the importance of considering  
432 more realistic and complex data when testing causal inference methods.  
433

#### 438 4.5 Impact of Undersampling on BOLD Signal in 439 fMRI Data

440 We also examined the effect of undersampling on time series data generated from a VAR model and then processed  
441 through a balloon model to simulate the BOLD response in fMRI data Buxton *et al.* [1998]. Given the smooth nature of  
442 the BOLD signal, undersampling by one-second intervals often leads to minimal information loss, while undersampling  
443 by larger intervals (e.g., two or three seconds) introduces significant inaccuracies. Figure 5 illustrates how different under-  
444 sampling rates impact the preservation of temporal information in BOLD data, underscoring that aggressive undersam-  
445 pling can obscure meaningful connectivity patterns.  
446

## 451 5 Conclusion

452 Undersampling is a critical yet often overlooked issue in the analysis of time series data, particularly in the context of  
453 fMRI. In this paper, we addressed the undersampling problem directly by incorporating its effects into the derivation of  
454 causal graphs using ASP. Our approach goes beyond traditional methods by explicitly accounting for the temporal dis-  
455 connect between neural processes and fMRI sampling rates.  
456 By doing so, we not only identified the most probable causal  
457 graph but also provided an equivalence class of potential  
458

graphs, enabling a more nuanced understanding of the underlying causal structures.  
461

Our results, validated on simulated fMRI data underscore the importance of addressing undersampling in neuroimaging studies. We demonstrated that our ASP-based method outperforms existing techniques, particularly in scenarios where undersampling distorts the true causal relationships between neural groups. Additionally, by comparing our approach to other algorithms, including those studied by Sanchez-Romero *et al.* [2019b], we highlighted that while methods like FASK show potential, they still fall short in fully capturing the complexities introduced by undersampling.  
462  
463  
464  
465  
466  
467  
468  
469  
470  
471  
472

The undersampling issue is not merely a technical challenge but a fundamental barrier to accurate causal inference in neuroscience. Ignoring it risks drawing erroneous conclusions about brain function and connectivity. Our work represents a significant advancement in this area, providing a robust and scalable solution that can improve the accuracy of causal inference in the presence of undersampling.  
473  
474  
475  
476  
477  
478  
479  
480  
481  
482  
483  
484

As the scientific community continues to explore the neural mechanisms underlying cognition and behavior, it is imperative that the undersampling problem is given the attention it deserves. Addressing this issue will be crucial in ensuring that the inferences drawn from fMRI data truly reflect the underlying neural dynamics, leading to more reliable and meaningful insights into brain function.  
485  
486  
487  
488  
489  
490  
491  
492  
493

## 6 Future Directions

One of the challenges of solving the optimization problem with ASP is the initial graph estimate  $\mathcal{H}$ . The estimation errors at the measurement time-scale may inflate the estimation errors at the causal timescale. However, simply selecting the estimator that minimizes the errors in  $\mathcal{H}$ , as we have done in this paper, may not be the optimal strategy. Not all errors in

494  $\mathcal{H}$  have the same effect on the quality of estimation and de-  
495 veloping methods that consider that interplay is a promising  
496 future direction.

497 Further optimization of the approaches to enable work with  
498 larger graphs may open potential new avenues of where our  
499 methods may be applied. Although, our presented approach  
500 is highly capable for working with reasonably sized graphs,  
501 extending the number of nodes by an order of magnitude  
502 could broaden the range of potential applications. This in-  
503 cludes futher practical application of the methods in the study  
504 of brain function via fMRI as well as other dynamic modalities.  
505

## 506 References

- 507 Mohmadsajad Abavisani, David Danks, and Sergey Plis.  
508 Grace-c: Generalized rate agnostic causal estimation via  
509 constraints. In *The Eleventh International Conference on  
510 Learning Representations*, 2023.
- 511 Lionel Barnett and Anil K Seth. Granger causality and trans-  
512 fer entropy are equivalent for gaussian variables. *Physical  
513 Review Letters*, 103(23):238701, 2009.
- 514 Steven L Bressler and Anil K Seth. Multivariate autoregres-  
515 sive modeling of fmri time series. *NeuroImage*, 19(2):361–  
516 375, 2003.
- 517 Richard B Buxton, Eric C Wong, and Lawrence R Frank.  
518 Dynamics of blood flow and oxygenation changes during  
519 brain activation: the balloon model. *Magnetic resonance  
520 in medicine*, 39(6):855–864, 1998.
- 521 David Danks and Sergey Plis. Learning causal structure from  
522 undersampled time series. In *NIPS Workshop on Causality*,  
523 volume 1, pages 1–10, 2013.
- 524 Olivier David, Isabelle Guillemain, Sandrine Saitlet, Se-  
525 bastien Reyt, Colin Deransart, Christoph Segebarth, and  
526 Antoine Depaulis. Identifying neural drivers with func-  
527 tional mri: an electrophysiological validation. *PLoS biol-  
528 ogy*, 6(12):e315, 2008.
- 529 Karl J Friston. Functional and effective connectivity in neu-  
530 roimaging: a synthesis. *Human brain mapping*, 2(1-2):56–  
531 78, 1994.
- 532 Kathleen M Gates and Peter C Molenaar. Group iterative  
533 multiple model estimation (gimme) for group-level  
534 structural equation modeling of fmri data. *NeuroImage*,  
535 42(2):416–426, 2010.
- 536 Martin Gebser, Benjamin Kaufmann, and Torsten Schaub.  
537 Conflict-driven answer set solving: From theory to prac-  
538 tice. *Artificial Intelligence*, 187:52–89, 2012.
- 539 Mingming Gong, Kun Zhang, Bernhard Schoelkopf,  
540 Dacheng Tao, and Philipp Geiger. Discovering tempo-  
541 ral causal relations from subsampled data. In *International  
542 Conference on Machine Learning*, pages 1898–  
543 1906. PMLR, 2015.
- 544 Clive WJ Granger. Investigating causal relations by econo-  
545 metric models and cross-spectral methods. *Econometrica:  
546 journal of the Econometric Society*, pages 424–438, 1969.
- 547 Daniel A Handwerker, John M Ollinger, and Mark  
548 D’Esposito. Variation of bold hemodynamic responses  
549 across subjects and brain regions and their effects on sta-  
550 tistical analyses. *Neuroimage*, 21(4):1639–1651, 2004.
- 551 Youngjun Kim, Juneyoung Lee, Woo-Seok Kim, Kangwook  
552 Lee, and Edward J Lee. Ec-gan: Estimating effective con-  
553 nectivity via generative adversarial networks. In *Proce-  
554 dings of the IEEE/CVF Conference on Computer Vision and  
555 Pattern Recognition (CVPR)*, pages 14131–14141, 2021.
- 556 Vladimir Lifschitz, Leora Morgenstern, and David Plaisted.  
557 Knowledge representation and classical logic. *Foundations  
558 of Artificial Intelligence*, 3:3–88, 2008.
- 559 Helmut Lütkepohl. *New introduction to multiple time series  
560 analysis*. Springer Science & Business Media, 2005.
- 561 Volodymyr Mnih, Adria Puigdomenech Badia, Mehdi Mirza,  
562 Alex Graves, Timothy Lillicrap, Tim Harley, David Silver,  
563 and Koray Kavukcuoglu. Asynchronous methods for deep  
564 reinforcement learning. *International Conference on Ma-  
565 chine Learning*, pages 1928–1937, 2016.
- 566 Joris M Mooij and Tom Claassen. Constraint-based causal  
567 discovery using partial ancestral graphs in the presence of  
568 cycles. In *Conference on Uncertainty in Artificial Intelli-  
569 gence*, pages 1159–1168. PMLR, 2020.
- 570 Roland Pamfil, Stefan Bauer, Natalia Díaz-Rodríguez, Bern-  
571 hard Schölkopf, and Jonas Peters. Dynotears: Structure  
572 learning from time-series data. *International Conference  
573 on Learning Representations*, 2020.
- 574 Subhrajit Paul, Prathosh AP Roy, and Deepali Jha. Amortiza-  
575 tion transformer for brain effective connectivity estimation  
576 from fmri data. In *Proceedings of the IEEE/CVF Confer-  
577 ence on Computer Vision and Pattern Recognition (CVPR)*,  
578 pages 17815–17824, 2022.
- 579 Judea Pearl et al. Models, reasoning and inference. *Cam-  
580 bridge, UK: Cambridge University Press*, 19:2, 2000.
- 581 Judea Pearl. *Causality*. Cambridge university press, 2009.
- 582 Sergey Plis, David Danks, Cynthia Freeman, and Vince Cal-  
583 houn. Rate-agnostic (causal) structure learning. *Advances  
584 in neural information processing systems*, 28, 2015.
- 585 Joseph D Ramsey, Stephen José Hanson, Catherine Hanson,  
586 Yaroslav O Halchenko, Russell A Poldrack, and Clark Gly-  
587 mour. Six problems for causal inference from fmri. *neu-  
588 roimage*, 49(2):1545–1558, 2010.
- 589 Thomas Richardson and Peter Spirtes. Ancestral graph  
590 Markov models. *The Annals of Statistics*, 30(4):962–1030,  
591 2002.
- 592 Jakob Runge, Peer Nowack, Marlene Kretschmer, Seth Flax-  
593 man, and Dino Sejdinovic. Detecting and quantifying  
594 causal associations in large nonlinear time series datasets.  
595 *Science Advances*, 5(11):eaau4996, 2019.
- 596 Mahdi Salehi, Hamid R Karimi, Soroush Honari, and Axel P  
597 Hill. Calltif: Whole-brain causal discovery using fmri data.  
598 In *Proceedings of the 30th International Joint Conference  
599 on Artificial Intelligence (IJCAI)*, pages 2078–2084, 2021.

- 600 Ruben Sanchez-Romero, Michael W Cole, and David M  
601 Schnyer. Estimating effective connectivity by jointly mod-  
602 eling neural dynamics and structural constraints. *NeuroIm-*  
603 *age*, 200:243–256, 2019.
- 604 Ruben Sanchez-Romero, Joseph D Ramsey, Kun Zhang,  
605 Madelyn RK Glymour, Biwei Huang, and Clark Glymour.  
606 Estimating feedforward and feedback effective connec-  
607 tions from fMRI time series: Assessments of statistical  
608 methods. *Network Neuroscience*, 3(2):274–306, 2019.
- 609 Anil K Seth, Paul Chorley, and Lionel C Barnett. Granger  
610 causality analysis of fmri bold signals is invariant to hemo-  
611 dynamic convolution but not downsampling. *Neuroimage*,  
612 65:540–555, 2013.
- 613 Shohei Shimizu, Patrik O Hoyer, Aapo Hyvärinen, and  
614 Marko Kerminen. A linear non-gaussian acyclic model for  
615 causal discovery. *Journal of Machine Learning Research*,  
616 7(Oct):2003–2030, 2006.
- 617 Stephen M Smith, Karla L Miller, Gholamreza Salimi-  
618 Khorshidi, Matthew Webster, Christian F Beckmann,  
619 Thomas E Nichols, Joseph D Ramsey, and Mark W Wool-  
620 rich. Network modelling methods for fmri. *Neuroimage*,  
621 54(2):875–891, 2011.
- 622 Peter Spirtes, Clark Glymour, and Richard Scheines. *Causa-*  
623 *tion, Prediction, and Search*. Springer New York, 1993.
- 624 Peter Spirtes, Clark N Glymour, Richard Scheines, and David  
625 Heckerman. *Causation, Prediction, and Search*. MIT  
626 press, 2000.
- 627 Peter Spirtes, Clark Glymour, and Richard Scheines. *Causa-*  
628 *tion, prediction, and search*. MIT press, 2001.
- 629 Pedro A Valdes-Sosa, Alard Roebroeck, Jean Daunizeau, and  
630 Karl Friston. Effective connectivity: influence, causality  
631 and biophysical modeling. *Neuroimage*, 58(2):339–361,  
632 2011.
- 633 Jiji Zhang. Causal reasoning with ancestral graphs. *Journal*  
634 *of Machine Learning Research*, 9:1437–1474, 2008.